On the estimation of the diffusion coefficient and distribution of hydrogen in stainless steel

Malo Duportal, Abdelali Oudriss, Xavier Feaugas, Catherine Savall

On the estimation of the diffusion coefficient and distribution of hydrogen in stainless steel

Malo Duportal*, Abdelali Oudriss*, Xavier Feaugas, Catherine Savall

*Corresponding authors: malo.duportal@univ-lr.fr ; abdelali.oudriss@univ-lr.fr

La Rochelle University, LaSIE UMR CNRS 7356, Av. Michel Crépeau, 17042 La Rochelle, France

Key words: *Austenitic steels, Stainless steel, Hydrogen Absorption, Hydrogen Diffusion, Kelvin Probe Force Microscopy*

Abstract

In this work, the localisation of hydrogen in an electrochemically charged stainless steel was investigated by Scanning Kelvin Probe Force Microscopy and Glow Discharge Optical Emission Spectroscopy analysis. Both techniques indicated a high hydrogen content at less than 90 micrometres under the charged surface. Thermal Desorption Spectroscopy was used to calibrate the data from both techniques and thus to calculate the hydrogen concentration. Finally, after assuming certain hypotheses, Fick's laws were used to calculate the coefficient of diffusion and subsurface concentration of hydrogen in cathodic charging conditions.

Stainless steel is widely used in many industrial sectors such as energy and transportation. However, in some situations steel can be exposed to aggressive environments which can lead to hydrogen embrittlement. Indeed, embrittlement results from the absorption of hydrogen through different processes, and the interaction of this solute with microstructural heterogeneities, coupled with mechanical stress can induce a fracture. The mechanisms associated with this phenomenon have been extensively studied and are mainly due to the interaction between hydrogen, the metallurgy of the metal and its defects together with the crystallographic structure [1-5]. However, these mechanisms are highly dependent on the diffusion and trapping of hydrogen. Indeed, stainless steel with a face-centred cubic structures (fcc) and a stable gamma phase has a low hydrogen diffusivity of between 10^{-13} and 10^{-15}m²/s at low temperatures (below 50°C) [6-8]. This makes a complete characterization (adsorption, absorption and diffusion) difficult with the usual electrochemical permeation. For this reason, experimental approaches based on techniques such as Tof-SIMS, NRA/ERDA, TDS, GDOES, etc. have been used to quantify hydrogen and to evaluate its distribution in a given microstructure, with some limitations [6, 9, 10]. Scanning Kelvin Probe Force Microscopy (SKPFM) is an alternative technic that can be used to study the distribution of hydrogen and to evaluate its apparent diffusion coefficient.

SKPFM is a non-contact, non-destructive technique, which is derived from Atomic Force Microscopy (AFM). SKPFM measures the local potential difference (CPD) between a conductive tip and a sample with a high resolution. Recent studies suggest that SKPFM is a promising tool to study hydrogen distribution in metals because of its ability to measure the variation of contact potential difference (CPD) after hydrogen absorption [11-16]. Indeed, it was shown that the surface work function could be affected by hydrogen [17]. For instance, distribution of hydrogen can be studied with a palladium layer, as hydrogen accumulation in the Pd layer induces a drop in the work function [18]. SKPFM showed that in duplex stainless steel, hydrogen has a higher solubility and lower coefficient of diffusion in austenite than in ferrite [19]. A recent study on SKPFM [20] demonstrated the grain orientation dependence of hydrogen diffusion in austenitic stainless steel. Larignon *et al.* used SKPFM to determine the gradient of hydrogen content after hydrogen absorption on aluminium alloy. In this

work, a correlation with Secondary Ion Mass Spectrometry (SIMS) analysis made it possible to discuss the SKPFM results on a surface with a native oxide film [14, 15]. Few studies have shown an increase in CPD after hydrogen absorption in austenitic stainless steel and nickel, which corresponds to a decrease in the work function [13, 21]. Additionally, Ma *et al.* [21] showed a partially reversible effect with hydrogen desorption on CPD.

In the present work, Scanning Kelvin Probe Force Microscopy (SKPFM) and Glow Discharge Optical Emission Spectroscopy (GDOES) experiments were performed on 316L specimens after cathodic charging. The combination of these two techniques proves the efficiency of SKPFM for hydrogen localisation in stainless steels. Additionally, the correlation with a measurement of total hydrogen concentration obtained by Thermal Desorption Spectroscopy (TDS) was used to quantify the hydrogen distribution below the surface of the charged specimens. Finally, SKPFM data analysis offers the opportunity to calculate an apparent diffusion coefficient using Fick's laws.

The material studied was a AISI 316L stainless steel (wt%): Cr 17.3, Ni 12.4, Mo 2.4, Mn 1.8, C 0.03, N 0.08 with an fcc austenitic microstructure which was characterized in a previous study [22]. The alloy is non-textured with an average grain size of 53µm. The samples were cylindrical with a diameter of 12mm and a thickness of 1mm. Specimens were embedded in epoxy resin and successively ground down to 4000 grit using SiC paper. They were then cleaned with ethanol prior to hydrogen charging on one side. Cathodic charging was used to introduce hydrogen into the alloy with a standard three-electrode set-up consisting of a saturated sulphate reference electrode (0.6513V/SHE), and a platinum grid as a counter electrode. The electrolyte solution was composed of $4g.L^{-1}$ NaOH (0.1M) and $3g.L^{-1}$ NH_4SCN (0.039M). Ammonium thiocyanate was used to promote hydrogen absorption [23]. The temperature was set at 50°C and the samples were exposed to a direct current of -100mA/cm². Total hydrogen concentration was measured using TDS (CGHE EMGA-621W from Horiba). For these analyses, the sample dimensions were $4x10x0.5mm^3$. Figure 1a shows the total concentration immediately after different charging times. The total hydrogen concentration increased with charging duration. Few differences were observed between 72h and 144h, the hydrogen concentration reached a steady stage which probably corresponds to maximum local solubility. These concentrations seem consistent with results obtained in previous studies under similar conditions [24]. Based on these results, two charging times were selected - 24h and 72h - giving 18±3wppm and 80±17wppm respectively (Figure 1). It is well known that hydrogen can diffuse into fcc material by migration from octahedral-tetrahedral-octahedral positions at room temperature [25, 26]. This diffusion induces hydrogen desorption which can be measured by TDS [10]. Figure 1b shows the hydrogen concentration during the desorption step after a charging time of 24h and 72h. The hydrogen concentration rapidly decreased during the first 48h and reached a plateau, which probably corresponds to trapped hydrogen with a concentration of 6±1 and 16±5wppm for 24h and 72h charged samples, respectively [10]. The other analyses presented here (SKPFM and GDOES) were performed at least 48h after H-charging, and thus on the desorption plateau at which the total H concentration did not change.

Figure 1: Hydrogen concentration of 316L *versus* charging time (a) and *versus* desorption time after charging (b).

SKPFM analyses were performed on cross sections as presented on the sketch in Figure 2-a. This method requires a high quality surface (low roughness and low strain hardening) so, after H-charging, the cross section was prepared and ground with diamond paste down to ¼µm and with a vibrating polisher (colloidal silica), ultrasonically cleaned in ethanol and dried in air (preparation time: 48h).

SKPFM measurements were performed in air at room temperature with an Agilent 5500LS apparatus from Keysight Technologies by single pass mode. Potential maps of 40µm by 40µm were successively

scanned from the charged surface to the bulk. A conductive tip (Si Pt/Ir coated from AppNano – ANSCM-Pt) was used and a Au-Si-Al reference sample (model: PFKPFM-SMPL) was scanned before each experiment as it has been reported that the CPD potential strongly depends on the experimental conditions (tip, surface preparation, humidity, acquisition parameters) [27]. For our system and our experimental conditions, the potential measured on the reference samples (Au and Al) were: $V_{CPD\text{-}Au} \approx$ -0.19±0.04V; $V_{CPD\text{-}Al} \approx$ 0.36±0.04V. The contact potential difference for a 316L uncharged sample was located around 0.30±0.06V. The final results are presented with a correction of the potential to bring the potential of the uncharged specimen to the same level, namely 0.3V. Figure 2 shows the CPD obtained by SKPFM on cross sections from the hydrogen entry surface to the exit surface on 316L charged 24h and 72h after a desorption time of at least 48h. The CPD for an uncharged specimen is also given as a reference. The CPD profiles presented in Figure 2a show a large increase on the charged surface. After a 72h charging, the CPD dropped to the bulk value at 70µm below the charged surface. After 24h charging, the CPD dropped to the bulk value for a transition distance of around 40µm.

Figure 2: SPKFM CPD profiles as a function of distance from the H-charged side for 316L samples (a) Charged 24h and 72h after a 2 day desorption (b) Charged 72h after a 2 and 9 day desorption

The measurements performed on the reference sample highlight the connection between the CPD and work function. In fact, when the work function increased (4.20eV for Al, and 5.47eV for Au [28]) the CPD decreased. Some authors have suggested that hydrogen ingress induces a decrease in the work function, which would result in an increase in the CPD [7, 13, 17]. These results imply that CPD profiles can reflect hydrogen distribution beneath the charging surface of a metal [14]. But the next question concerns hydrogen detection on a metallic oxide surface due to passive layer formation.

Few studies have given a physical interpretation for the drop in the SKPFM CPD with hydrogen in steel [12, 29-32]. A possible interpretation draws on the fact that hydrogen induces a reduction of Fe^{3+} to Fe^{2+} in a native oxide film [12]. Moreover, two other studies conducted by SKP measurement on bare steel samples [33] and pure iron foils [16], found that the work function of iron is determined by the Fe^{2+}/Fe^{3+} ratio in the oxide. In fact, this ratio should modify the band structure of the oxide and the Fermi level position. However, many more factors may affect CPD, such as the formation of vacancies and defective oxide structures [34].

In order to confirm the correlation between the CPD profile and hydrogen distribution, GDOES analyses (Profiler-2 Horiba) were performed with a 4mm anode by sputtering the surface with argon ions (14W at 850Pa), with an abrasion speed of around 1.75µm.min^{-1}.

Figure 3a shows the GDOES hydrogen profiles for an uncharged specimen and for a charged specimen after 11 days of desorption. It is obvious that the hydrogen signal was much more intense after H-charging. It was verified that, after H-charging, the GDOES profiles of the metallic elements (Fe, Cr, Ni and S) were not significantly modified. C and O signals for the same samples were checked (Figure 3b) and were similar for charged and uncharged samples. Moreover, the hydrogen signal of the non-charged sample faded rapidly, as did the carbon and oxygen profiles. This suggests that the GDOES hydrogen profile for the uncharged sample corresponds to surface contamination. In contrast, for the charged sample, the decrease in the hydrogen signal was much slower than that of the C and O signals. This proves that after H-charging and desorption at ambient temperature, hydrogen is detected up to 60µm to 90µm under the charging surface, well below the contamination layer. Moreover, the thickness of the region containing hydrogen is in good agreement with the KFM CPD profile of Figure 2b for the 72h hydrogen charged sample.

Figure 3: GDOES profiles of a charged and an uncharged sample a) for hydrogen b) for carbon and oxygen.

GDOES supports the previous results obtained with SKPFM, confirming that the CPD drop seems to be correlated with hydrogen localisation. The influence of charging time on the CPD profiles (Figure 2a) is in good agreement with the TDS results as increasing the charging time led to higher hydrogen content. Figure 2b shows the CPD profiles for a 72h charged sample after 2 and 9 days of desorption. The profile was slightly wider after 9 days, but hydrogen distribution was not greatly modified between 2 and 9 days of desorption.

The drop in CPD for a 72h hydrogen charged sample was large (around 500mV), compared with a drop of less than 160mV obtained on an aluminium alloy by Larignon *et al* [14]. These differences can be explained by the effects of the materials, oxide properties and hydrogen concentration, which differ between the two alloys. The penetration of hydrogen in a 316L obtained by SKPFM was not as high as in aluminium alloy [14]. Actually, the diffusion coefficient of hydrogen is significantly different in these two materials (between 10^{-11}-10^{-14}m²/s for aluminium [14] alloy and 10^{-13}-10^{-15}m²/s for austenitic stainless steels [6-8]). In addition, charging conditions and especially charging temperature can strongly influence hydrogen ingress. For instance, here hydrogen charging was conducted at 50°C whereas a temperature of 150°C was used for the above-mentioned results obtained on aluminium.

The diffusion coefficient D can be calculated from a gradient of concentration C(x) along a direction x perpendicular to the surface of hydrogen ingress [35]. SKPFM and GDOES profiles were used here to evaluate this parameter. Assuming the hydrogen desorption follows a Fick's law in a semi-infinite solid, the surface concentration is constant and for a material without any trap sites, we obtain [35]:

$$C(x) = C_s\left(1 - \mathrm{erf}\left(\frac{x}{2\sqrt{Dt}}\right)\right) \quad (1)$$

where C(x) is the species concentration at a given distance, C_s is the surface concentration, x is the distance from the surface (m), D is the coefficient of diffusion (m²/s) and t is the charging time (s).

A second hypothesis is that the concentration of hydrogen is proportional to the CPD potential or the GDOES signal over the bulk [6, 36, 37]. With this assumption it is possible to introduce a corrective factor k, which converts the concentration in SKPFM or GDOES signals S:

$$S(x) = \mathrm{C}(x).\mathrm{k} \quad (2)$$

where k is the corrective factor and S(x) the fitting signal at a given distance (SKPFM or GDOES).

Figure 4: SKPFM (a) and GDOES (b) calculated profiles and experimental signals of a 72h hydrogen charged sample after several days of desorption corrected by an uncharged sample signal.

Figure 4 present the calculated SKPFM and GDOES profiles, respectively, compared to the experimental profiles. The uncharged sample signals were subtracted from the experimental profiles. According to McKibben *et al.* [35], at the end of H-charging, assuming the hydrogen profile is controlled by diffusion, the surface concentration instantaneously drops to zero and the concentration profile exhibits a maximum. Therefore, only the signal after the peak was fitted with equation (1). Two informations can be deduced from these simulations, namely the apparent diffusion coefficient and the surface concentration of hydrogen (Cs). Total hydrogen concentration measured by TDS after 72h charging on a sample of 500µm was 80±17wppm. Given the results, hydrogen seemed to be localized 76µm above the charged surface, which corresponds to a mean concentration of approximately 526wppm within those 76µm. First, the curvature of the fitted plot is adjusted by calculating the diffusion coefficient (eq. 1 and 2). Then, the corrective factor (k) was calculated (using the area of the curves and hydrogen concentration) and this was used to determine a surface

concentration of 1863wppm from the SKPFM. This corresponds to an occupation of 10.4% of the available octahedral sites. The surface concentration obtained from the GDOES and SKPFM profiles are in good agreement (respectively 1680wppm and 1863wppm). The equivalent hydrogen pressure (P_{H2}) associated with the hydrogen charging conditions considered in the present work can be estimated (9.7×10^5atm.) from Sievert's law:

$$C_s(\text{wppm}) = 33.1.\sqrt{P_{H2}}.\exp(-11080/RT) \quad (3)$$

with R the gas constant ($J.K^{-1}$ mol^{-1}), T the temperature (K) and P_{H2} the hydrogen pressure (atm.) [24].

A 72h charged sample gave an apparent diffusion coefficient of 1.4 $.10^{-15}m^2/s$ and 2.2 $.10^{-15}m^2/s$ by SKPFM and GDOES, respectively. These results are in good agreement with those obtained using the Arrhenius law developed in two other studies [13, 24] for a 304 and a 316L austenitic stainless steel, which gave 1.7 $.10^{-15}m^2/s$ and 1.3 $.10^{-15}m^2/s$, respectively, at 50°C (which corresponds to the charging temperature used in our work). Chen *et al.* have already performed permeation tests on austenitic stainless steel at 10°C with Devanathan-Stachurski cells and obtained an apparent coefficient of diffusion of between 1.0-3.2 10-15m²/s for a similar steel composition [8].

To sum-up, TDS, SKPFM and GDOES provided a robust method to analyse hydrogen distribution after cathodic charging in an austenitic stainless steel. The distribution was used to calculate an approximate coefficient of diffusion using Fick's laws (1.4 $10^{-15}m^2/s$), which is in good agreement with the data in the literature.

Acknowledgments

This work was supported by the Ministère de l'Enseignement Supérieur et de la Recherche. The GDOES experiment was performed at the CRM Group (*Avenue du Bois Saint-Jean 21 P59 4000 Liège BELGIQUE*) - our thanks to C. Brandt and A. Dupont. The authors wish to thank P. Jacques and S. Reuter from the pole IMAP of the Catholic University of Louvain-la-Neuve (*Place Sainte Barbe 2/L5.02.02 1348 Louvain-la-Neuve*) for helpful discussions. We would also like to acknowledge our colleagues C. Berziou and R. Milet for their contributions to the TDS facilities in our laboratory.

References

[1] G. Pressouyre, Metall. Trans. A. 10 (1979) 1571
[2] R. Kirchheim, Prog. Mater. Sci. 32 (1988) 261
[3] A. Turnbull, Int. J. Hydrogen Energy 40 (2015) 16961
[4] F. Martin, X. Feaugas, A. Oudriss, D. Tanguy, L. Briottet et J. Kittel, «8 - State of hydrogen in Matter:Fundamental Ad/Absorption, Trapping and Transport Mechanisms,» in Mechanics - Microstructure - Corrosion Coupling, Editor(s): Christine Blanc, Isabelle Aubert, Elsevier, 2019, pp. 171-197.
[5] G. Hachet, J. Li, A. Hallil, A. Metsue, A. Oudriss, J. Bouhattate and X. Feaugas, Eng. Fract. Mech. 218 (2019)
[6] P. Kumar and R. Balasubramaniarn, J. Alloys Compd. 255 (1997) 130
[7] Y. Huang, F. Xuan, S.-T. Tu and T. Itoh, Mater. Sci. Eng., A 528 (2011) 1882
[8] Y. Chen, D. Santos and C. Sequeira, Defect and diffusion forum, 258-260 (2006) 322
[9] A. Oudriss, J. Creus, J. Bouhattate, E. Conforto, C. Berziou, C. Savall and X. Feaugas, Acta Mater. 60 (2012) 6814
[10] A. Oudriss, F. Martin and X. Feaugas, "11 - Experimental Techniques for Dosage and Detection of Hydrogen," in Mechanics - Microstructure - Corrosion Coupling, Editor(s): Christine Blanc, Isabelle Aubert, Elsevier, 2019, pp. 245-268
[11] S. Evers, C. Senöz and M. Rohwerber, Electrochim. Acta 110 (2013) 534
[12] S. Evers, C. Senöz and M. Rohwerder, Sci. Technol. Adv. Mater. 14 (2013) 014201
[13] Z. Hua, S. Zhu, B. An, T. Iijima, C. Gu and J. Zheng, Scr. Mater. 162 (2019) 219

[14] C. Larignon, J. Alexis, E. Andrieu, L. Lacroix, G. Odemer and C. Blanc, Scr. Mater. 68 (2013) 479
[15] C. Larignon, J. Alexis, E. Andrieu, L. Lacroix, G. Odemer and C. Blanc, Electrochim. Acta 110 (2013) 484
[16] A. Nazarov, F. Vucko and D. Thierry, Electrochim. Acta 216 (2016) 130
[17] M. Rohwerder and C. Benndorf, Surf. Sci. 307-309 (1994) 789
[18] S. Evers and M. Rohwerder, Electrochem. Commun. 24 (2012) 85
[19] M. Li, L. Guo, L. Qiao and Y. Bai, Corros. Sci. 60 (2012) 76
[20] Z. Hua, B. Anb, T. Iijima, C. Gu and J. Zheng, Scr. Mater. 131 (2017) 47
[21] Z. Ma, X. Xiong, L. Zhang, Z. Zhang, Y. Yan and Y. Su, Electrochem. Commun. 92 (2018) 24
[22] X. Feaugas and C. Gaudin, Int. J. Plast. 20 (2004) 643
[23] E. Akiyama and S. Li, Corros. Rev. 34 (2015) 23
[24] A. Brass and J. Chêne, Corros. Sci. 48 (2006) 3222
[25] E. Wimmer, W. Wolf, J. Sticht and P. Saxe, Phys.Rev. B 77 (2008) 134305
[26] A. Metsue, A. Oudriss et X. Feaugas, Corrosion 75 (2019) 898
[27] C. Örnek, C. Leygraf and J. Pan, Corros. Eng., Sci. Technol., 54 (2019) 185
[28] D. Lide, CRC Handbook of Chemistry and Physics 12-124, CRC Press, 2005
[29] C. Senöz, S. Evers, M. Stratmann and M. Rohwerder, Electrochem. Commun. 13 (2011) 1542
[30] J. Yu, J. Luo and P. Norton, Electrochim. Acta, 47 (2002) 1527
[31] J. Yu, C. Zhang, J. Luo and P. Norton, J. Electrochem. Soc., 150 (2003) B68
[32] S. Modiano, J. Carreño, C. Fugivara, R. Torresi, V. Vivier, A. Benedetti and O. Mattos, Electrochim. Acta 53 (2008) 3670
[33] M. Rohwerder and F. Turcu, Electrochim Acta 53 (2007) 290
[34] D. Zang, P. Maroevic and R. McLellan, J. Phys. Chem. Solids 60 (1999) 1649
[35] R. McKibben, R. Sharp, D. Harrington, B. Pound and G. Wright, Acta Metall. 35 (1987) 253
[36] T. Roy, R. Balasubramaniam and A. Ghosh, Scr. Mater. 34 (1996) 1425
[37] A. Barnoush and H. Vehoff, Scr. Mater. 55 (2006) 195

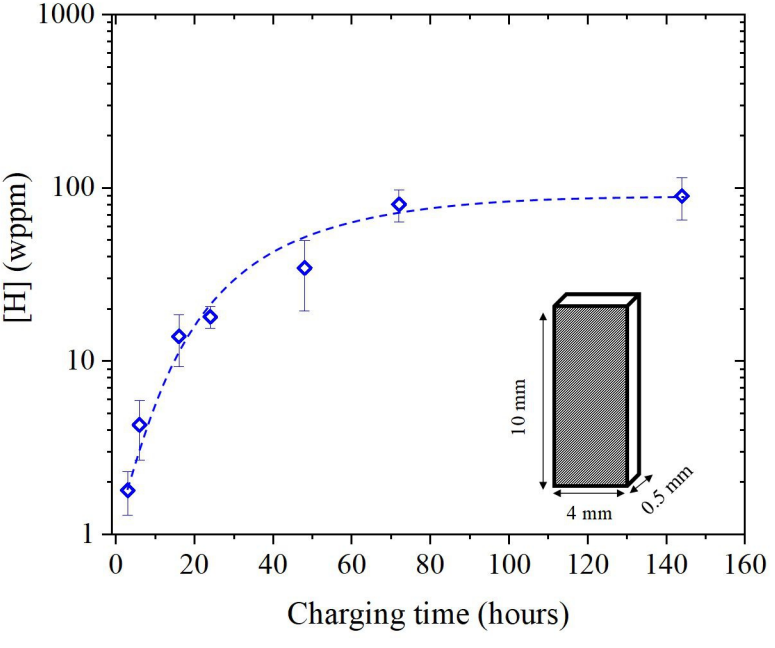
1000
100
10
1
[H] (wppm)
0
20
40
60
80
100
120
140
160
Charging time (hours)
10 mm
4 mm
0.5 mm

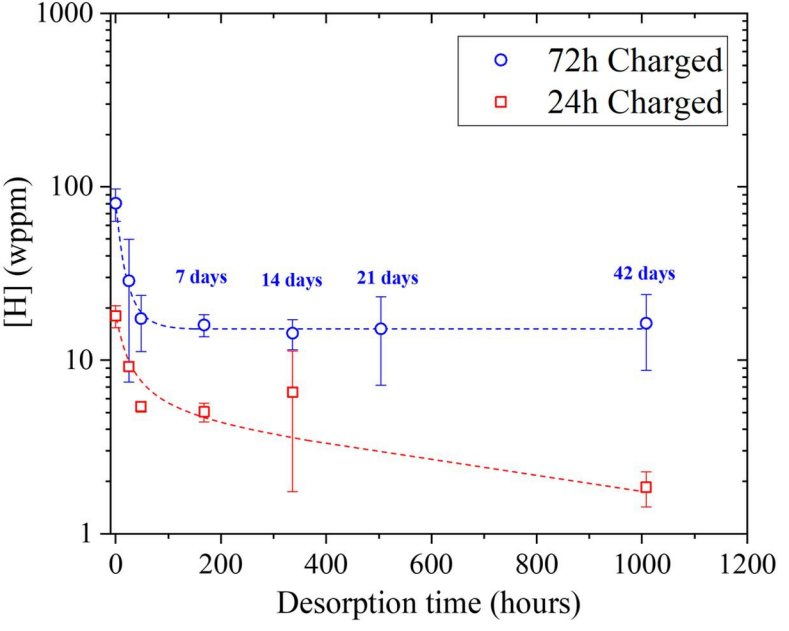
1000
100
10
1
[H] (wppm)
0
200
400
600
800
1000
1200
Desorption time (hours)
72h Charged
24h Charged
7 days
14 days
21 days
42 days

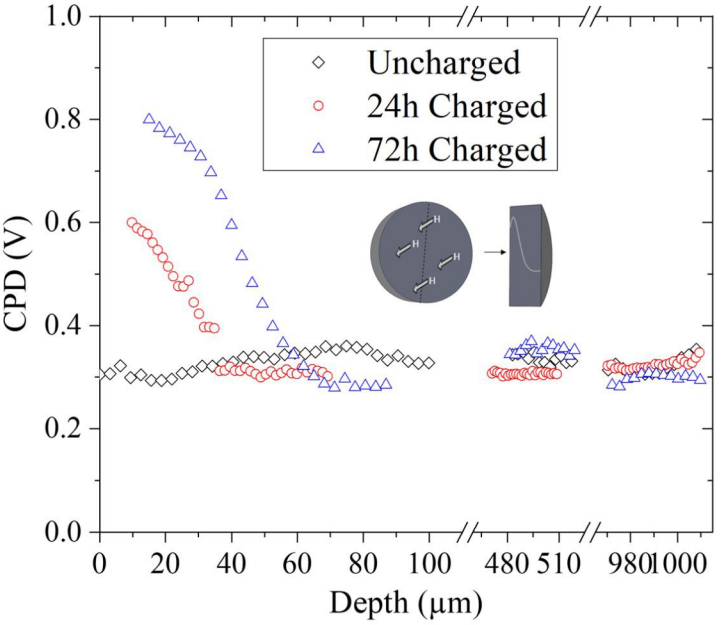
Uncharged
24h Charged
72h Charged
CPD (V)
Depth (μm)
1.0
0.8
0.6
0.4
0.2
0.0
0
20
40
60
80
100
480
510
980
1000
H

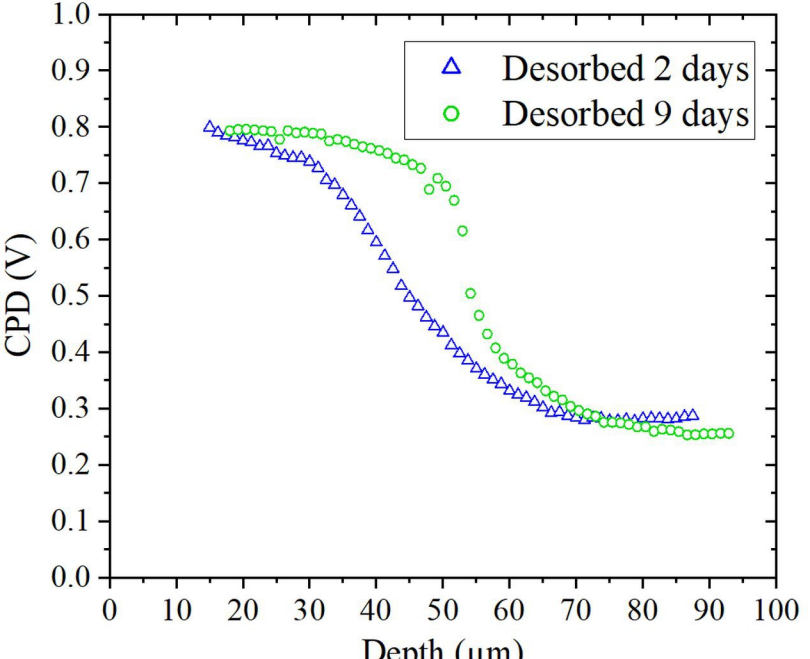
Desorbed 2 days
Desorbed 9 days
CPD (V)
Depth (μm)
1.0
0.9
0.8
0.7
0.6
0.5
0.4
0.3
0.2
0.1
0.0
0
10
20
30
40
50
60
70
80
90
100

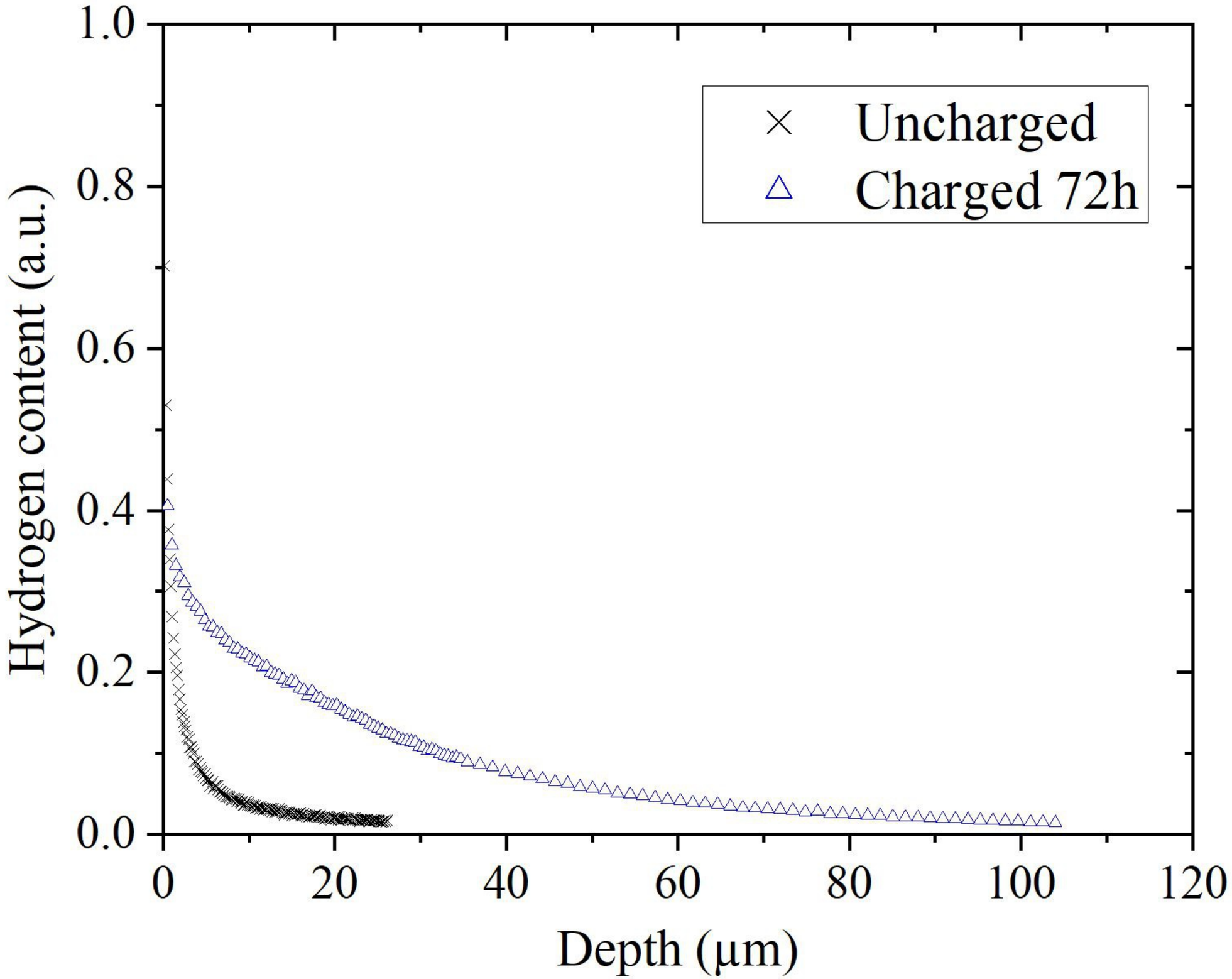
Uncharged
Charged 72h
Hydrogen content (a.u.)
1.0
0.8
0.6
0.4
0.2
0.0
0
20
40
60
80
100
120
Depth (μm)

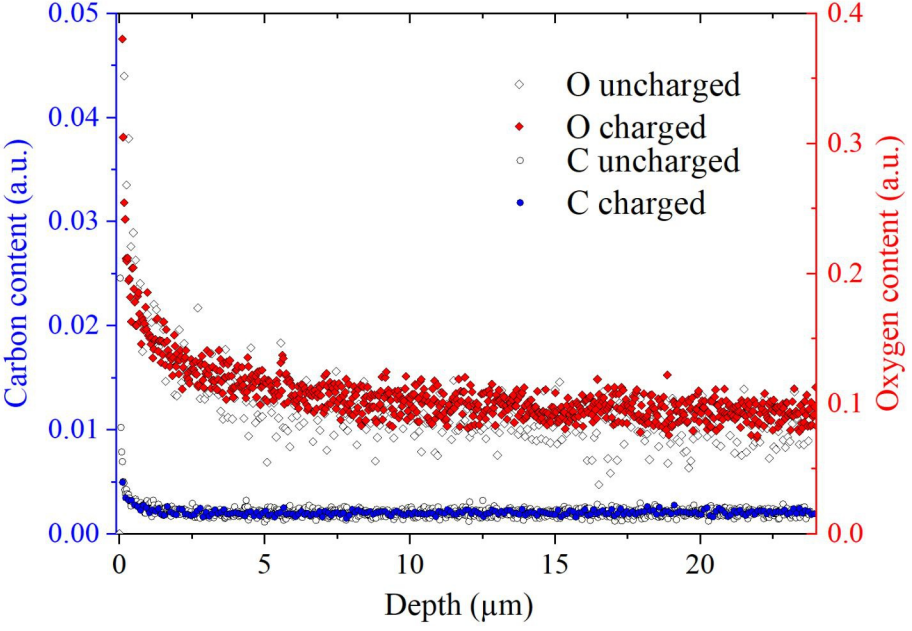
0.05
0.04
0.03
0.02
0.01
0.00
Carbon content (a.u.)
0.4
0.3
0.2
0.1
0.0
Oxygen content (a.u.)
O uncharged
O charged
C uncharged
C charged
0
5
10
15
20
Depth (μm)

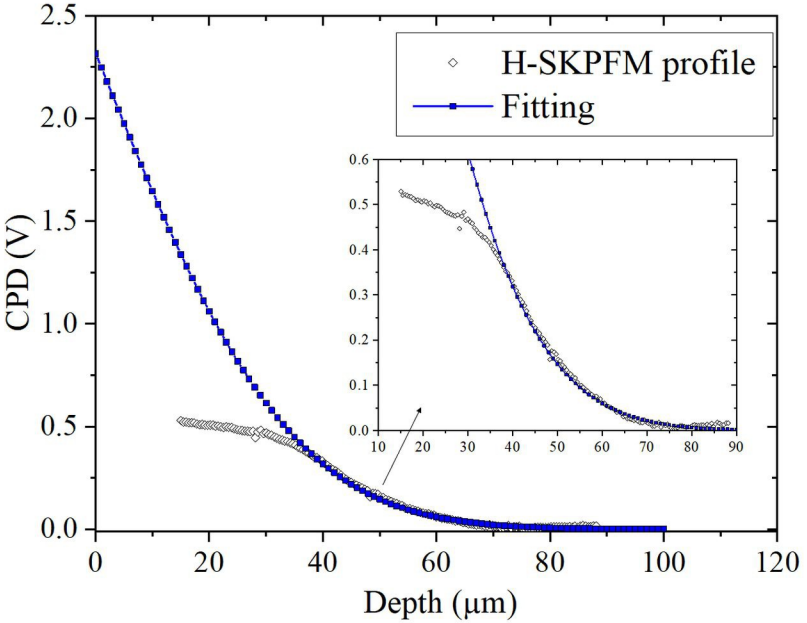
H-SKPFM profile
Fitting
CPD (V)
Depth (μm)
2.5
2.0
1.5
1.0
0.5
0.0
0
20
40
60
80
100
120
0.6
0.5
0.4
0.3
0.2
0.1
0.0
10
20
30
40
50
60
70
80
90

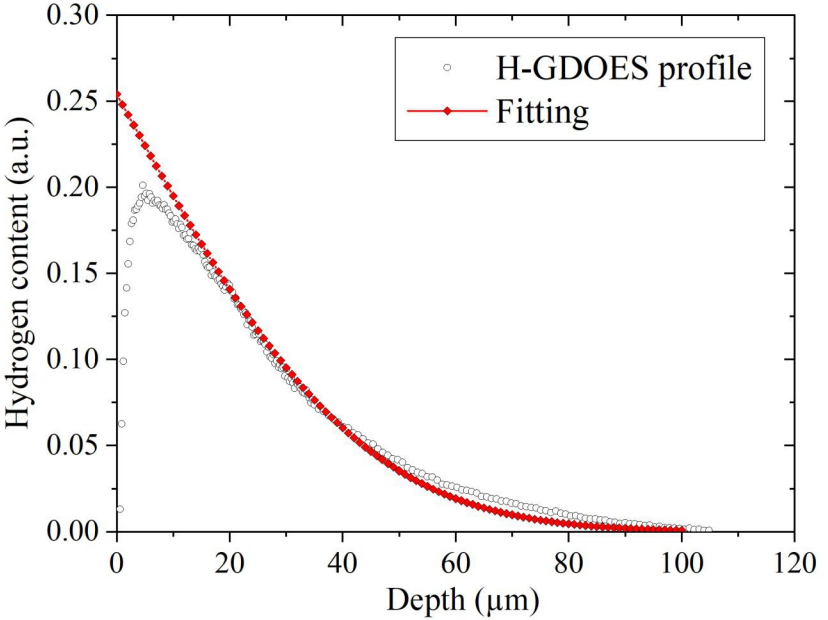
H-GDOES profile
Fitting
Hydrogen content (a.u.)
Depth (μm)
0.00
0.05
0.10
0.15
0.20
0.25
0.30
0
20
40
60
80
100
120

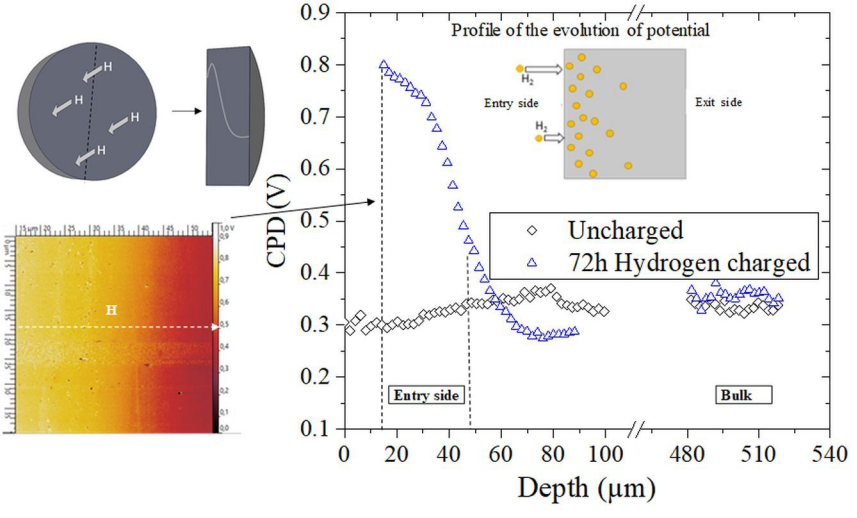
H
H
H
H
H
H
Profile of the evolution of potential
H_2
Entry side
Exit side
H_2
Uncharged
72h Hydrogen charged
CPD(V)
Entry side
Bulk
Depth (μm)
0.9
0.8
0.7
0.6
0.5
0.4
0.3
0.2
0.1
0
20
40
60
80
100
480
510
540